scientific reports

OPEN

Tumor microenvironment modulation by SERPINE1 increases radioimmunotherapy in murine model of gastric cancer

Javeria Zaheer[1,2], Joycie Shanmugiah[1,2], Seungyoun Kim[1,2], Hyeongi Kim[1] & Jin Su Kim[1,2✉]

An elevated extracellular matrix (ECM) and interstitial fluid pressure (IFP) in gastric cancer limits the targeting of HER2-expressing cells when radioimmunotherapy (RIT) with ^{64}Cu-trastuzumab (^{64}Cu-TRZ) is utilized. Here, we used Losartan (LOS) to downregulate ECM and IFP in gastric cancer mice model. In our study we treated the gastric cancer mice model with a dose of 40 mg/kg of LOS. We found that the LOS treatment increases a twofold higher Alexa-647-TRZ accumulation which significantly enhanced ^{64}Cu-TRZ. We determined that the LOS-treated samples exhibited reduced mRNA and protein expression of SERPINE1, a gene associated with the ECM degradation. Additionally, LOS treatment resulted in the downregulated mRNA expression of the TGF-β1 and COL13A1, the genes involved in ECM deposition and an upregulated RNA expression of MMP2, a gene associated with the ECM degradation. There were no significant changes in metastatic markers of N-Cadherin and E-Cadherin. Moreover, our study demonstrates that silencing SERPINE1 increases the activity of the MMP2 and decreases COL13A1 with no effect on the N-cadherin and E-cadherin were observed. Our novel combinational therapy of using ^{64}Cu-TRZ with LOS is attributed to the downregulation of SERPINE1 targeting ECM and IFP is highly effective for treatment of gastric cancer.

Keywords Trastuzumab, ^{64}Cu, Losartan, Radioimmunotherapy, Extracellular matrix, SERPINE1

Abbreviations

LOS	Losartan
TRZ	Trastuzumab
ECM	Extracellular matrix
IFP	Interstitial fluid pressure
COL	Collagen
^{64}Cu-TRZ	^{64}Cu-trastuzumab
^{64}Cu-TRZ + LOS	^{64}Cu-trastuzumab plus LOS
PET	Positron emission tomography
COL13A1	Collagen XIII type A1
MMP	Matrix metalloproteinase
TGFβ1	Transforming growth factor beta 1
AT1R	Angiotensin receptor blocker
RIT	Radioimmunotherapy
AUC	Area under curve
OCT	Optimal cutting temperature compound

Gastric cancer is a leading cause of cancer-related deaths worldwide. The 2017 global disease burden data showed 1.22 million incidences of gastric cancer worldwide and 848,000–885,000 individuals with reported cancer-related death[1]. HER-2 is overexpressed in approximately 22% of gastric cancer patients[2].

Trastuzumab (TRZ), a recombinant humanized anti-HER-2 monoclonal antibody, is a treatment option for patients with HER2-positive advanced gastric cancer[2]. Radioimmunotherapy (RIT) exploits monoclonal antibodies (mAbs) as radionuclide-labeled antibodies that explicitly bind to tumor antigens[3]. RIT was developed

[1]Division of Applied RI, Korea Institute of Radiological and Medical Sciences, 75 Nowon-Ro, Nowon-Gu, Seoul 01812, Republic of Korea. [2]Radiological and Medical Sciences, University of Science and Technology (UST), Seoul 01812, Republic of Korea. ✉email: kjs@kirams.re.kr

1

by labelling ^{64}Cu (t$_{1/2}$, 12.7 h, β + (655 keV, 17.4%) and β- (573 keV, 39.0%)) with TRZ for PET imaging and achieving the therapeutic effect for cancer[4].

The clinical application of RIT for solid tumors including gastric cancer is limited by the extracellular matrix (ECM) barrier[3,5,6]. The ECM, increased cellularity and desmoplasia can hinder drug transport in tumor tissues[7–9]. Collagen, the major component of ECM materials, is the primary matrix molecule responsible for the inhibition of drug transport Collagen functions as a physical barrier that prevents antitumor drug transport, penetration, and diffusion, which results to lessen the efficacy of RIT[8–10].

Gastric cancer has widely distributed ECM components, tightly packed cells, and elevated interstitial fluid pressure, which encumber RIT transport to target gastric cancer[4]. The deposition of the ECM was associated with poor prognosis and therapy response in gastric cancer[11] Modifiers such as collagenase[12], hyaluronidase[13] and matrix metalloproteinases 1 and 8[14] have been used to degrade ECM.

Strategic practices are needed to overcome the ECM barrier and achieve the desired therapeutic response to RIT in gastric cancers. During RIT with ^{64}Cu-TRZ for solid tumors, the surrounding normal tissue is at a risk of radiation damage. Therefore, a deeper and more uniform distribution of ^{64}Cu-TRZ is important[15]. ^{64}Cu undergoes three distinct modes of transmutation: positron decay, beta decay, and electron capture. These transformations result in the emission of positrons for imaging through positron emission tomography (PET) and β- for therapeutic applications. Utilizing ^{64}Cu for PET imaging allows for the assessment of biodistribution and pharmacokinetics of substances, including mAbs. ^{64}Cu and ^{67}Cu were isotopes of each other, so they share same chemical properties, allowing us to predict the targeting of ^{67}Cu therapy based on the distribution of ^{64}Cu.

Losartan (LOS), an angiotensin receptor blocker (AT1R), and has been approved by the Food and Drug Administration (FDA) as an antihypertensive drug that controls vascular tension and is commonly prescribed to hypertensive patients[7]. In our study we aimed to investigate the potential of LOS combination therapy to enhance the uptake of RIT while minimizing the side effect compared to the combination therapy with chemotherapeutics. We hypothesized that LOS could enhance the efficacy of RIT by promoting ECM degradation and reducing IFP, thereby improving its target domain. In addition to evaluating the impact of RIT, we examined the target gene to gain insight into the underlying mechanism.

Results

Losartan reduces ECM components and drops the interstitial fluid pressure

We conducted experiments to evaluate the impact of LOS on ECM components in gastric cancer. We stained collagen and ECM polysaccharides, which are the major components of ECM. Masson trichrome staining (Fig. 1A) showed that LOS significantly reduced collagen. We observed 30% reduction in %collagen content (Fig. 1B). Alcian blue staining (Fig. 1C) showed that LOS significantly reduced ECM polysaccharides. We observed 39% reduction in %ECM polysaccharide (Fig. 1D). The anesthetized mice underwent needle-guided transducer insertion directly into the tumor. This was followed by retraction of the needle and placement of the transducer probe into the tumor tissue (Fig. 1E). Remarkably, LOS treatment led to a significant 60% reduction in IFP compared to the control group (Fig. 1F). In the control group, the pressure ranged from a minimum of 58.02 mmHg to a maximum of 91.02 mmHg. However, with LOS treatment, the pressure range decreased to a minimum of 15.8 mmHg and a maximum of 38.07 mmHg.

Losartan delayed tumor growth, and improved survival rate

We conducted cytotoxicity assessment of LOS in our study. The NCI-N87 cells treated with LOS exhibited an increased in propidium iodide staining, indicating cell death. Furthermore, the cell viability of the 3D-cultured N87 cancer cells significantly decreased to 69% viability upon treatment with 40 µM of LOS. We also observed significant cell cycle arrest in the G0/G1 phase (**Fig. S1A**) Therapeutic efficacy showed delayed tumor growth in LOS treated sample (Fig. 1G) and increased the survival rate compared with the control (Fig. 1H). The median survival times were 30.5 days, 37.5 days for the control and LOS treated groups, respectively. The cell cytotoxicity with 3D culture cells shows significant cytotoxic effect to 69% at 40 µM LOS treatment (Fig. 1I).

Losartan enhanced therapeutic effect of trastuzumab

Due to the high expression of ECM, including collagen and ECM polysaccharides, TRZ penetration into the tumor core was restricted. We investigated whether the addition of LOS increased TRZ penetration into the tumor tissues. To evaluate the effects of LOS, we injected Alexa-647-TRZ (150 µg/100 µL, n = 5) with 40 mg/kg LOS (n = 5). Alexa-647-TRZ binding to the HER2 receptor was shown in **Fig. S1B.** The experimental schedule was shown in **Fig. S1C.**

Figure 2A showed representative images of Alexa-647-TRZ (top) and in combination with LOS (bottom). The area under the curve (AUC) from both the vessel (Fig. 2B) and edge regions (Fig. 2C) were significantly improved after LOS treatment (***P < 0.001). Total uptake Alexa-647 conjugated TRZ across the entire tumor section was also enhanced after LOS treatment (**P < 0.005) as shown in Fig. 2D. There was no significant difference in IFP between the LOS and LOS plus TRZ groups. Images of the tumor tissue are presented in **Fig. S2A.** We observed delayed tumor growth (Fig. 2E) and increased survival rate in the LOS plus TRZ group compared to the TRZ group (Fig. 2F). Increased penetration was not limited to TRZ only. We also observed increased tissue micro distribution of atezolizumab from ex-vivo tumor tissue imaging of HapT1 pancreatic cancer (golden hamster), U87 MG glioblastoma (BALB/c nude), CT26 colon cancer (BALB/c) and A549 lung cancer (BALB/c nude), rituximab in raji lymphoma (SCID mice), cetuximab in U87 MG glioma (BALB/c nude), A549 lung cancer (BALB/c nude) and CT26 colon cancer (BALB/c) cell line based tumor xenografts with LOS treatment as shown in Fig. 2G.
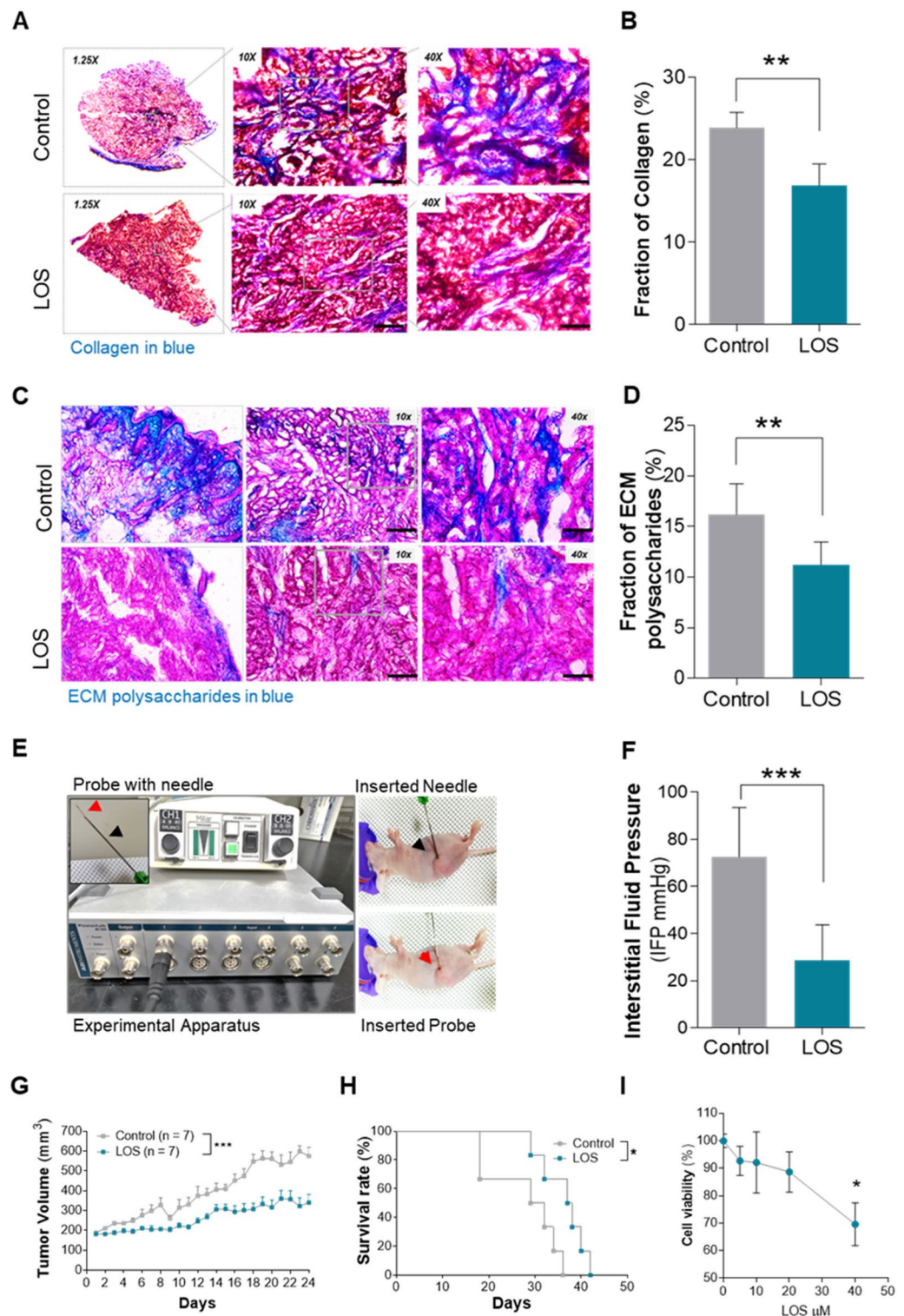
Fig. 1. LOS degrades extracellular matrix including collagen and ECM polysaccharide and reduces interstitial fluid pressure (IFP) (n = 5). (**A-D**) Representative image of collagen and ECM polysaccharides stained in blue for control and LOS-treated sample and fraction of collagen content and ECM polysaccharides quantification (above left Magnification: × 12.5, × 100, and × 400. (**E**) Experimental apparatus for measuring IFP and (**F**) IFP measurement between LOS and control presented as mm Hg. (**G-H**) Tumor volume and survival. Data are considered statistically significant where P value is less than 0.05. One way Anova test and the log-rank (Mantel-Cox) test was performed to compare tumor volume and the survival rates. * Denotes $P < 0.05$, ** denotes $P < 0.005$, *** denotes $P < 0.001$, where NS means non-significant.
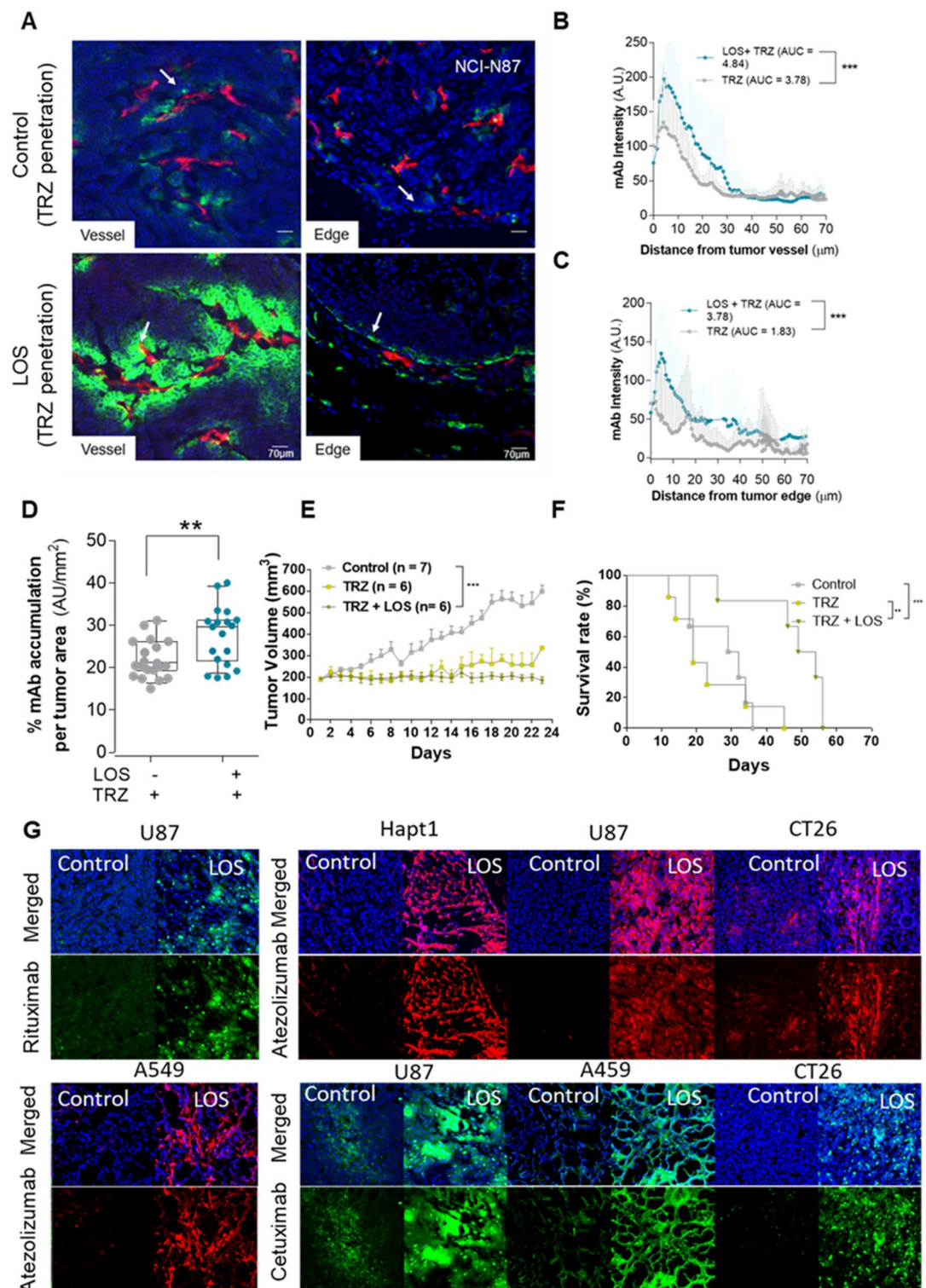
Fig. 2. Losartan (LOS) enhances trastuzumab (TRZ) accumulation across tumor tissues (n = 5). (**A**) Representative fluorescent images obtained from in cell microscopy show DAPI in blue, TRZ (Alexa-647-TRZ) in green, and vessel in red (lectin) in the TRZ alone and TRZ plus LOS (TRZ + LOS) groups. Arrow indicates extravasated TRZ. (**B**) Quantification analysis of TRZ and TRZ plus LOS accumulation from the tumor vessel (**C**) and tumor edge. (**D**) Quantification analysis of the TRZ (green signal) across tumor tissue sections (n = 20) in each group via MIPAV software. Scattered bar graph with mean line with error bar as standard derivation (S.D) are shown (** P < 0.005). (**E–F**) Tumor volume and survival. (**G**). Therapeutic monoclonal antibody penetration in different models. The data are statistically significant, and the error bars are represented above each data point as standard deviation. One way Anova test and the log-rank (Mantel-Cox) test was performed to compare tumor volume and the survival rates. * denotes $P < 0.05$, ** denotes $P < 0.005$, *** denotes $P < 0.001$, where N.S means non-significant.

Losartan enhanced uptake and therapeutic effect of ^{64}Cu-Trastuzumab

To evaluate the potential of combinational ^{64}Cu-TRZ with LOS, we performed PET imaging of the NCI-N87 xenograft mice model with ^{64}Cu-TRZ or ^{64}Cu-TRZ with LOS. The experimental schedule for PET/CT imaging is shown in **Fig. S1C.** PET scanning was performed for up to five days after the first injection (Fig. 3A). ^{64}Cu-TRZ with LOS showed a significantly increased the standard uptake value (SUV) compared with ^{64}Cu-TRZ on days 4 and 5 as shown in Fig. 3B. The IFP of ^{64}Cu-TRZ with LOS was significantly reduced compared with that of ^{64}Cu-TRZ alone and the control (Fig. 3C). Next, we evaluated the therapeutic response to combination treatment with TRZ and LOS. ^{64}Cu-TRZ with LOS delayed the tumor growth compared to ^{64}Cu-TRZ (Fig. 3D). The percent median survival of ^{64}Cu-TRZ with LOS was improved compared to both ^{64}Cu-TRZ alone and to control (Fig. 3E). Individual tumor volumes for PBS, LOS-treated, TRZ-treated, TRZ + LOS treated, ^{64}Cu-TRZ treated, and ^{64}Cu-TRZ + LOS treated are presented in **Fig. S2B**, where for comparison a single plot is shown for all groups (**Fig. S2C**). Dose absorption for normal organ and tumor was shown in **Table. S1**. The tumors treated with ^{64}Cu-TRZ had an absorbed dose of 139.46 ± 48.95 mGy/MBq whereas the tumors treated with ^{64}Cu-TRZ with LOS had an absorbed dose of 209.0 ± 16.52 mGy/MBq.

Losartan targets ECM by downregulating SERPINE1 but does not directly influence the metastasis

QuantSeq analysis was performed to identify changes in mRNA expression in control and LOS-treated tumor tissues. Volcano plots for DEG for the LOS-treated samples are colored in blue (**Fig. S4A).** Among the significant changes in gene expression, we observed a notable 0.15-fold-downregulated mRNA expression of SERPINE1 in LOS-treated samples (**$P < 0.005$). Gene interaction analysis showed that SERPINE1 interacted with collagen type XIII alpha 1 chain (Col13A1) and matrix metalloproteinase-2 (MMP2) in **Fig. S4B**. The mRNA SERPINE1 level after LOS treatment were confirmed by the qPCR as shown in Fig. 4A. Furthermore, the qPCR analysis also revealed the changes in the mRNA expression of TGF-β as in Fig. 4B

SERPINE1 has been identified as a cancer-promoting gene in gastric adenocarcinoma[16]. High expression of SERPINE1 is significantly related to poor prognosis in gastric adenocarcinoma[17]. We demonstrated that ex-vivo SERPINE1 expression was significantly downregulated following LOS treatment Fig. 4C. The total intensity of SERPINE1 per tumor area in the immunofluorescence images was significantly decreased Fig. 4D. And the western blotting (*$P < 0.05$, Fig. 4E-F) confirmed the reduced protein expression of SERPINE1 gene in the corresponding ex-vivo tissue samples. QuantSeq analysis of tumor tissue showed 1.39-fold upregulation of MMP2 (*$P < 0.05$). qRT-PCR confirmed the 0.17-fold downregulation of COL13A1 gene in tumor tissue with LOS (*$P < 0.05$, Fig. 4G). qRT-PCR confirmed that both MMP2 (*$P < 0.05$, Fig. 4H) and total MMP (**$P < 0.005$, Fig. 4I), which were significantly increased in ex-vivo tumor tissues. Since LOS modulation of ECM can indirectly influence some aspects of the metastasis, however, there was no change of the metastatic markers such as N-cadherin and E-cadherin as confirmed by Quantseq and qRT-PCR (Fig. 4J-M).

Silencing SERPINE1 in conjunction to LOS treatment targets ECM and IFP

In our study, we employed Lipofectamine-mediated transfection of NCI-N87 cells with siRNA targeting SERPINE1 to examine the therapeutic potential of the downregulating SERPINE1 in conjunction with LOS treatment. We first confirmed the reduced expression of the SERPINE1 in NCI-N87 cells by LOS. Immunofluorescence staining of LOS-treated cells showed significantly low SERPINE1 expression as compared to control (***$P < 0.001$) in **Fig. S5A**. Upregulated total MMP were observed in-vitro cell supernatant (*$P < 0.05$) in **Fig. S5B**. Silencing of SERPINE1 against siRNA SERPINE1 for three primer sequences is confirmed by RT-PCR as shown in Fig. 5A. Additionally, we compared the tumor pattern between PBS, LOS, siSERPINE1 and scramble RNA as negative control (NC) in **Fig. S5C**. We observed no significant change in collagen in the knee joints, determined by Safranin O staining (*$P < 0.05$, **Fig. S5D**). Silencing SERPINE1 gene in N87 cells we observed 0.59-fold, 0.53-fold and 0.24-fold downregulation of COL13A1 in three primer sequence (*$P < 0.05$, Fig. 5B) and a fivefold increase of MMP2 in Fig. 5C and 1.4-fold increase in total MMP from the cell supernatant as determined by MMP assay kit (*P < 0.05, Fig. 5D). Although the levels of both MMP2 and total MMP are increased, there were no changes in either N-cadherin or E-cadherin (Fig. 5E-F). A decreased IFP was observed with siSERPINE1 group compared to that of control (**$P < 0.005$, Fig. 5G). Given the role of SERPINE1, we further investigated whether its inhibition could influence RIT distribution. To assess its impact, we employed siSERPINE1 treatment, which involves the use of small interfering RNA (siRNA) to specifically downregulate SERPINE1 expression at the post-transcriptional level. PET/CT scans were conducted at 24 and 48 h post-injection of ^{64}Cu-DOTA-Trastuzumab in mice treated with siSERPINE1 or NC, and effect of siSERPINE1 on the RIT distribution was shown in **Fig. S3.** TCGA data from the human protein atlas showed high expression of SERPINE1 as a prognostic factor in gastric cancer (***$P < 0.001$, Fig. 5H).

Discussion

In our study, we aimed to investigate the therapeutic efficacy of RIT in combination with LOS and the mechanism underlying ECM degradation following LOS treatment. We made several important findings, shedding light on the connection between SERPINE1 and ECM degradation, which has not been previously explored in gastric cancer. We observed that the LOS treatment leads to the degradation of ECM, as indicated by the reduced level of ECM components and drops the IFP was shown in Fig. 1F. Figure 1G illustrates that during the initial 2–4 days, there was no significant difference in tumor size between the LOS treatment group and the control. This suggests that LOS requires sufficient time to degrade the ECM effectively. Since the half-life of ^{64}Cu was only 12.8 h, it did not provide enough time for the enhanced therapeutic effect of ^{64}Cu-TRZ due to LOS-induced ECM degradation. Therefore, the difference of SUV between the ^{64}Cu-TRZ and ^{64}Cu TRZ + LOS groups could be observed at relatively later time points, specifically at 96 and 120 h.
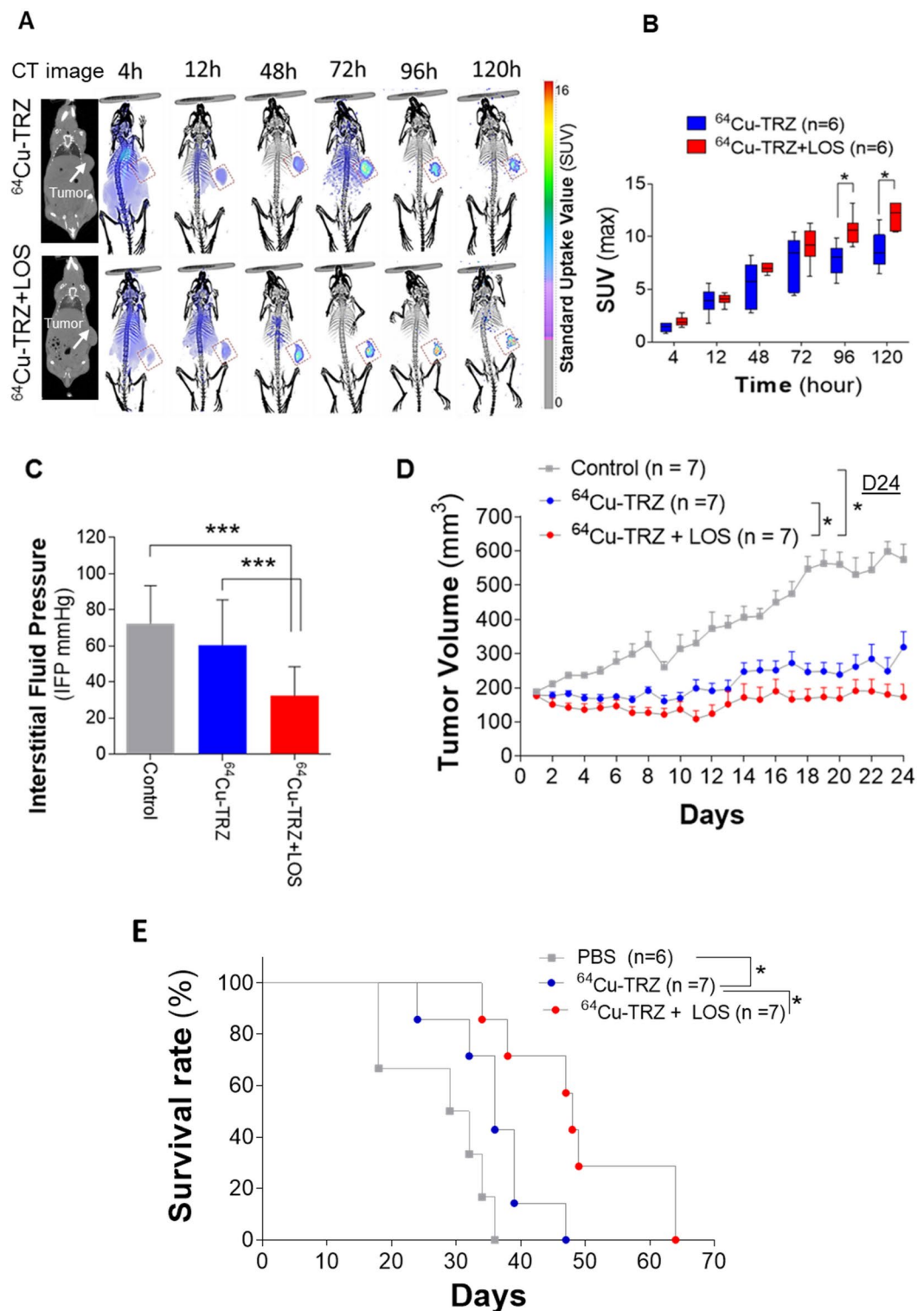
Fig. 3. ImmunoPET images of ^{64}Cu-TRZ and ^{64}Cu-TRZ with LOS uptake in gastric cancer. (**A**) Representative PET/CT images of ^{64}Cu-TRZ and ^{64}Cu-TRZ with LOS at subsequent time interval at 4 h, 12 h, 48 h, 72 h, 96 h, and 120 h. (**B**) Standard uptake value (SUV) for each time point (n = 6). (**C**) Interstitial pressure (**D-E**) Tumor volume and survival. One way Anova test and the log-rank (Mantel-Cox) test was performed to compare tumor volume and the survival rates. * denotes $P < 0.05$, ** denotes $P < 0.005$, *** denotes $P < 0.001$, where NS means non-significant.
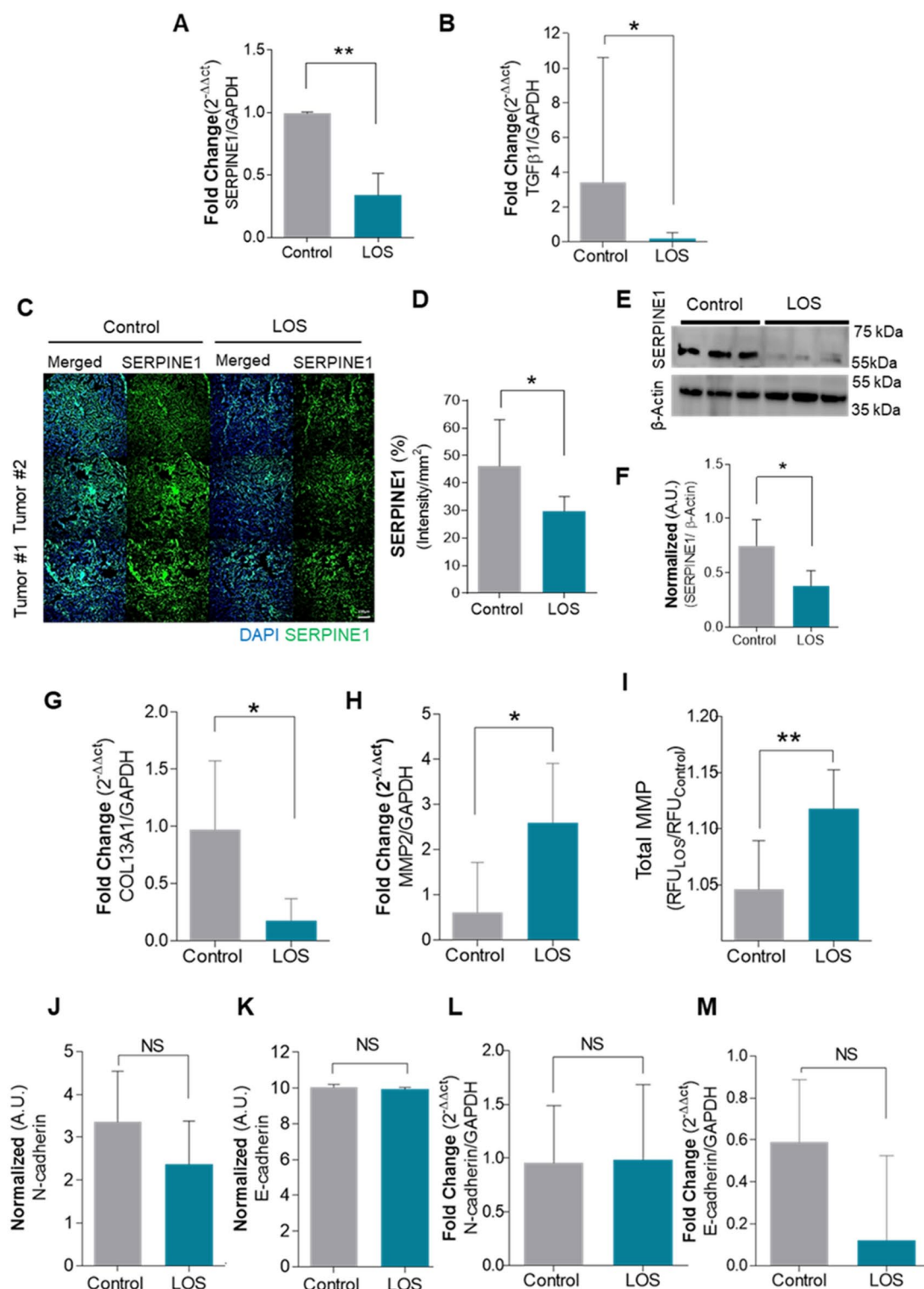
Fig. 4. LOS targets ECM by downregulating SERPINE1 (n = 3). (**A**) qRT-PCR shows mRNA level of SERPINE1. (**B**) TGF-β. (**C**) Ex-vivo tumor tissue for immunofluorescence shows reduced fluorescent signal for SERPINE1 in LOS treated tumor tissue compared to control. **D.** Signal intensity quantification for SERPINE1. (**E–F**) Western blot and quantification. (**G**) qRT-PCR shows mRNA level of COL13A1 and (**H**) MM2 where (**I**) shows the ex-vivo total protein level of MMPs. (**J**) Quant Seq normalized data for N-cadherin, (**K**), and E-cadherin and (**L**), qRT-PCR expression of N-cadherin and (**M**), E-cadherin shows no significant difference with LOS treatment. A two-tailed student's t-test was used. * denotes $P < 0.05$, ** denotes $P < 0.005$, *** denotes $P < 0.001$, where NS means non-significant.
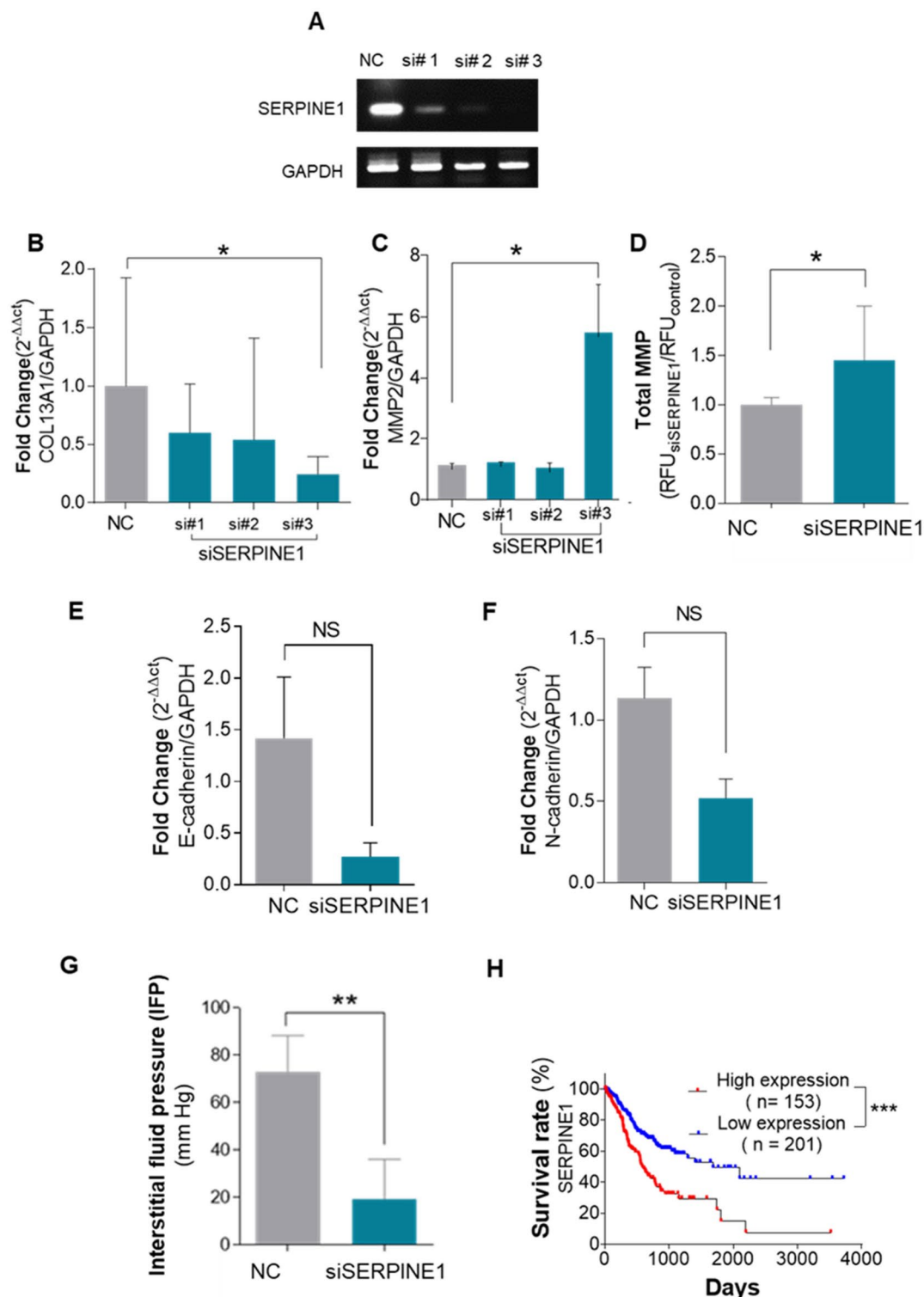
Fig. 5. Silencing SERPINE1 downregulates collagen type XIIIA1 and increases MMP activity (n = 3). (**A**) Silenced SERPINE1 gene expression among three different sequencing primers via qRT-PCR and (**B**) qPCR for Collagen type XIIIA1 and for (**C**) MMP2 gene. (**D**) MMP activity assay for total MMP activity (**E–F**) E-cadherin and N-cadherin for siSERPINE1. (**G**) Interstitial fluid pressure (IFP) of siSERPINE1 and negative control. (**H**) TCGA data shows higher expression of SERPINE1 is prognosis. The human protein atlas shows survival data for high expression and low expression of SERPINE1 gene in gastric cancer. The cut-out points of 24.7 FPKM. P score < 0.05. Data are considered statistically significant where P value is less than 0.05. A two-tailed student's t-test was used. * denotes $P < 0.05$, ** denotes $P < 0.005$, *** denotes $P < 0.001$, where NS means non-significant.

Because the gastric cancer has widely distributed ECM components, tightly packed cells, and elevated interstitial fluid pressure, which encumber RIT transport to target gastric cancer [4]. LOS treatment has shown to alleviate these factors by improving the targeting of HER2 antigen by facilitating the micro distribution of monoclonal antibody across the tumor tissue as shown in Fig. 2. In addition, LOS improved the therapeutic efficacy of ^{64}Cu-TRZ in gastric cancer (Fig. 3). We analyzed the biodistribution of their mAB with and without LOS and described the difference in the SUV parameter in the tumor.

The suppression of SERPINE1 expression by losartan demonstrated the connection between extracellular matrix (ECM) remodeling and improved therapeutic outcomes, particularly in the context of reducing tumor interstitial pressure and enhancing the efficacy of radioimmunotherapy (RIT). The inhibition of SERPINE1 by losartan, which was confirmed through multiple experimental approaches such as QuantSeq analysis, qPCR, and immunofluorescence, may lead to a shift in ECM dynamics. This enhanced ECM degradation, driven by the upregulation of MMPs such as MMP2, reduced the mechanical resistance within the tumor microenvironment, which in turn lowered tumor interstitial pressure. High interstitial pressure is known to limit the penetration of therapeutic agents, including radioimmunoconjugates used in RIT. By decreasing the interstitial pressure, losartan-induced suppression of SERPINE1 facilitated better blood flow and improved distribution of the therapeutic agents, thereby increasing the efficacy of RIT. Furthermore, gene interaction analysis (Fig. S4B) revealed that SERPINE1 was connected with ECM components, including collagen type XIIIA1 (COL13A1). LOS treatment led to the downregulation of COL13A1 (Fig. 4G). SERPINE1 silencing also reduced COL13A1 expression (Fig. 5B).

MMP activity is responsible for ECM hydrolysis and collagen degradation[18].MMP2 cleaves the Gly-ile/ Leu bond in collagen α chains[19]. We observed increased MMP2 expression via qRT-PCR and elevated total MMP activity in tumor tissue samples following LOS treatment (Fig. 4) and SERPINE1 gene silencing in vitro (Fig. 5). Additionally, we found similar pattern of tumor growth between siSERPINE1 and LOS treated tumor as shown in **Fig. S5C**. TGF-β acts as a pro-metastatic factor in advanced cancer[20,21]. We found LOS-induced downregulation of TGF-β, could possibly inhibit cancer metastasis. The lack of alteration of N-cadherin, E-cadherin and downregulation of TGF-β (Fig. 4) may play a role in the inhibition of metastasis. After depletion of ECM components, possible side effects include degradation of collagen in the knee joints. However, we found no observable change in knee joint of mice by safranin O stain (**Fig. S5D**).

The IFP is a fundamental metric in cancer biology. A high IFP is associated with a low tumor penetration of diagnostic mAbs[22]. Elevated tumor pressure affects the efficacy of other cancer treatments and causes the heterogeneous intratumoral distribution of drugs and macromolecules[23]. The interstitial pressure within the tumor region can be decreased using anticancer drugs[24]. If the osmotic pressure gradient is relatively constant throughout the tumor, a reduction in IFP may enhance antibody delivery from the tumor periphery[25]. Paclitaxel treatment[26] or high-intensity focused ultrasound[27] increased the accumulation of B3 mAb in tumors after the decrease of IFP and the loss of integrity in the tumor tissue[27,28]. In our study, LOS degraded the ECM, which induced a decrease in the IFP which could enhanced uptake of ^{64}Cu-TRZ or TRZ. IFP is regulated by the interaction between stromal cells and the extracellular matrix. This regulation facilitates the transport of nutrients and maintains the mechanical properties of the soft tissue[28,29]. Many solid tumors showed elevated IFP. This was due to multifactorial causes, such as abnormal leaky vasculature, lymphatic vessel drainage, or solid stress induced by compact cells to the cell junction and the extracellular matrix. Elevated ECM anchors on the filaments that reside on stromal cells which elevate the interstitial pressure and are observed to be an obstacle to drug delivery. Lowering the IFP increases drug delivery[24,30,31]. Moreover, collagenase degraded collagen content and decreases IFP while improving drug delivery[12]. Thus, measuring the IFP could predict the phenomenon of ECM reshaping. In this study, we showed that lowering the IFP modulates the ECM and enhances the interstitial transport of TRZ in gastric cancer. Collagen and ECM polysaccharides were reduced in LOS-treated tumor tissues and IFP was lowered in LOS-treated tissue, additionally LOS treatment shows cytotoxic effect (Fig. 1). Consequently, we observed a decrease in tumor volume and an improved survival rate (Fig. 1G-H). The decreased tumor volume could be explained by the reduced ECM component (Fig. 1A), decreased IFP (Fig. 1E-F) and cytotoxic effect of LOS (Fig. 1I). The results indicated that the combinational RIT of ^{64}Cu-TRZ with LOS could have improved therapeutic potential compared to ^{64}Cu-TRZ alone. According to the result of dosimetry, treatment with LOS showed a reduced organ dose absorption and increased tumor dose. The tumors treated with ^{64}Cu-TRZ had an absorbed dose of 139.46 ± 48.95 mGy/MBq whereas the tumors treated with ^{64}Cu-TRZ with LOS had an absorbed dose of 209.0 ± 16.52 mGy/MBq (**Table. S1**). A reduced IFP significantly improved the microdistribution of TRZ within the tumor in LOS-treated samples. Enhanced fluorescent conjugated TRZ was observed not only from the vessels but also from the tumor edge in LOS-treated tissues (Fig. 2). The increased of mAb was not limited to TRZ only. We also observed increased penetration of therapeutic mAb like rituximab, cetuximab, atezolizumab (Fig. 2G). Because of the recent advent of high linear energy transfered α-particle (such as ^{211}At (t$_{1/2}$, 7.2 h), ^{213}Bi (t$_{1/2}$, 46 min), ^{225}Ac (t$_{1/2}$, 10 days), and ^{233}Ra (t$_{1/2}$, 11 days)), α-particle labeled RIT would be a more promising potential therapeutic agent used in oncology[5]. We compared the absorbed dose using ^{64}Cu, ^{67}Cu and α emitters such as ^{211}At, and ^{225}Ac. The expected absorbed dose (mGy/MBq) with ^{64}Cu, ^{67}Cu, and ^{225}Ac was 136.47 ± 48.96, 174.33 ± 61.13, $14,930.00 \pm 5264.76$, $35,200.00 \pm 12,374.57$, respectively. The results indicated that the absorbed dose was increased when α particle was used (**$P < 0.005$). In terms of treatment, when using ^{64}Cu, we were unable to achieve a sufficient RIT therapeutic effect. However, when using α particles, it can be expected that the absorbed dose in the tumor will be at least 10 times higher. Therefore, the results of this study will be helpful in using ^{211}At-TRZ or ^{225}Ac-TRZ to enhance the therapeutic effect of RIT with α particles in the future. In particular, for α particles, with a range of less than 100 μm, strategies to degrade the ECM within the tumor are expected to be more beneficial (Fig. 6).

The purpose of this study was to identify the underlying mechanisms of LOS to degrade ECM. Although the energy of ^{64}Cu was lower than that of α-particle, ^{64}Cu-TRZ provided both immunoPET and RIT at the same
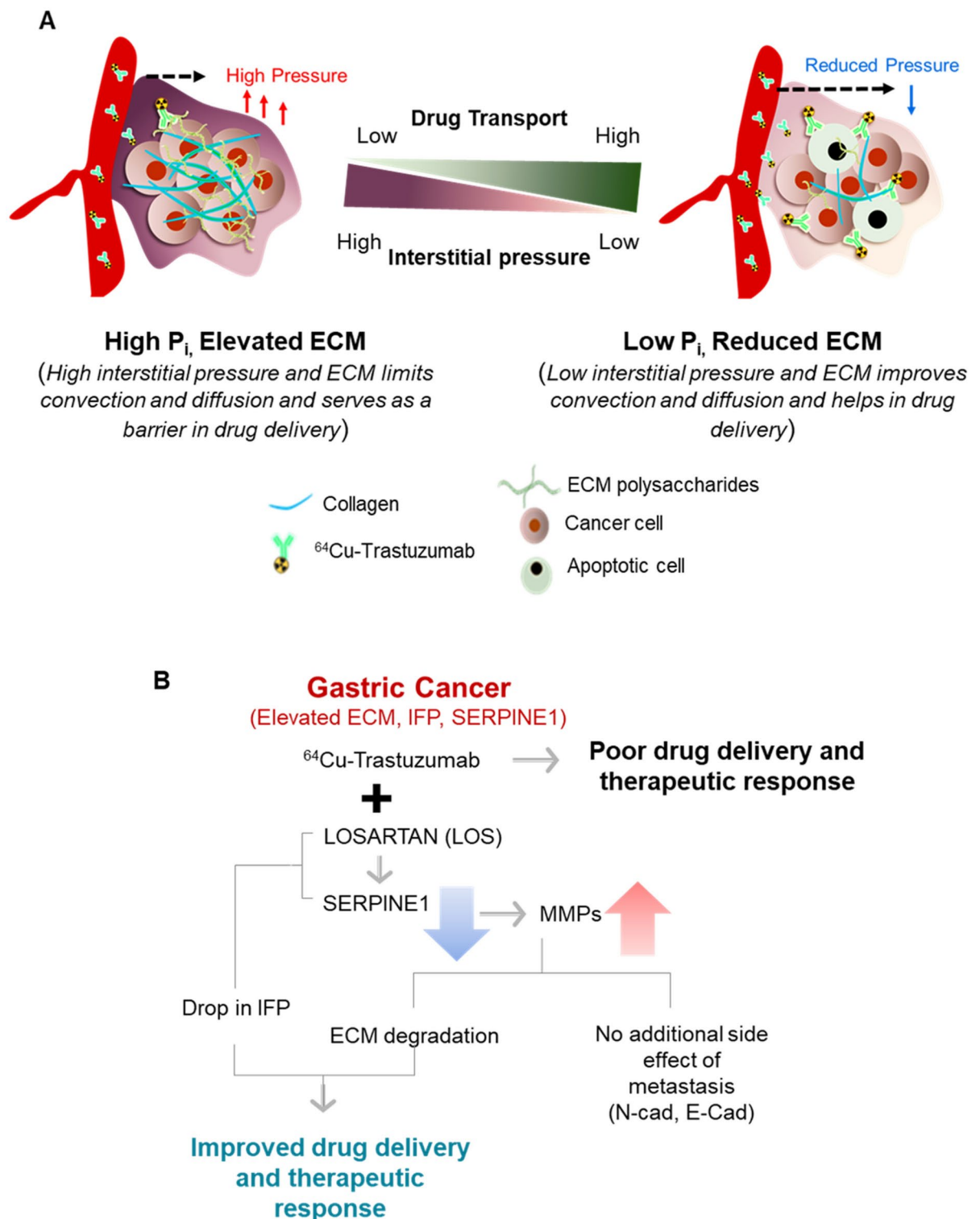
Fig. 6. A schematic representation illustrating how SERPINE1 downregulation modulates the tumor microenvironment to enhance the therapeutic efficacy of radioimmunotherapy in a murine model of gastric cancer.

time and ^{64}Cu-TRZ plus LOS showed sufficient tumor regression (Fig. 3). Further, If LOS combination therapy and α particle RIT was performed, greater therapeutic effects can be expected. LOS delayed tumor growth could be an apoptotic effect of LOS as observed via increased propidium iodide stain, cell cytotoxicity with 3D culture cells and cell cycle arrest at G0/G1 phase were observed in LOS treated sample (**Fig. S1**).

In light of recent developments, new SERPINE1 inhibitors like VHH-s-a03 have emerged[32]. VHH-s-a03 could also serve as a potential candidate for boosting the effectiveness of RIT.

In summary, our findings indicated that LOS treatment has a substantial impact on the ECM components of gastric cancer. It reduces collagen content, decreases ECM polysaccharides, and significantly lowers IFP within the tumor microenvironment by downregulation of SERPINE1. Thus, the enhanced effectiveness of ^{64}Cu-TRZ in gastric cancer treatment was observed. Our suggested combination RIT strategy holds promise for enhancing the therapeutic efficacy in gastric cancer treatment.

Materials and methods

Animal care
All animal experiments were performed in accordance with the institutional guidelines of the Korea Institute of Radiology and Medical Sciences (KIRAMS) and the protocols were approved by the Institutional Animal Care and Use Committee (IACUC number: KIRAMS 2020–0027). BALB/c nude male mice (Shizuoka Laboratory Center, Japan) (n = 6–7 for individual studies) were 5–6 weeks old at the start of the experiment. The animals were weighed, caged, housed, and maintained for 24 h in a light/dark cycle.

Cell culture
The NCI-N87 HER2-positive gastric cancer cell line was obtained from the American Type Culture Collection (ATCC). The culture medium comprised of 1% antibiotics (Sigma, St. Louis, MO, USA) and 10% fetal bovine serum (FBS, corning, USA). The cells in Roswell Park Memorial Institute (RPMI 1640 (corning, USA)) medium were maintained at 37 °C in a humidified 5% CO_2 incubator.

Cell viability with 3D culture
To investigate the cytotoxicity of TRZ and LOS, 3D-cultured cells were prepared, and the cell viability assay was performed using the alamarBlue® assay (Thermo Fisher Scientific, Waltham, MA, USA) following the manufacturer's instructions. Briefly, spheroids were initiated by seeding NCI-N87 at 5000 cells/well in ultra-low attachment 96-well plates with U-shaped wells (Corning, NY, USA), followed by centrifugation for 15 min at 4 °C and 1200 rpm and incubation until the spheroids grew to the appropriate size in a medium containing 10% FBS and 1% penicillin/streptomycin at 37 °C in 5% CO_2 (typically at least 3 days). The spheroids were then treated with TRZ 5 μg/mL in PBS, and/or 40 μM LOS in PBS. Cell viability was measured at an excitation wavelength of 560 nm and an emission wavelength of 590 nm using a microplate reader (i3X, Molecular Devices, USA). The emission values were expressed as percentages of controls, yielding the percentage cell viability after 48 h of treatment with TRZ and/or LOS.

Gastric Cancer xenograft model
NCI-N87, a HER2-positive gastric cancer cell line, was obtained from ATCC and maintained at the Roswell Park Memorial Institute (RPMI). It was processed by adding 10% fetal bovine serum with 5% antibiotics (Sigma, St. Louis, MO, USA) and maintained at 37 °C in a humidified CO_2 incubator. Tumor xenografts were prepared by the subcutaneous injection of NCI-N87 cells (5×10^6 cells/100μL).

QuantSeq analyses

RNA isolation
Total RNA was isolated using TRIzol reagent (Invitrogen). RNA quality was assessed using an Agilent 2100 bioanalyzer and an RNA 6000 Nano Chip (Agilent Technologies, Amstelveen, The Netherlands) (n = 3) and RNA quantification was performed using an ND-2000 Spectrophotometer (Thermo Inc., DE, USA).

Library preparation and sequencing
For control and test RNAs, library construction was performed using the QuantSeq 3' mRNA-Seq Library Prep Kit (Lexogen, Inc., Austria) according to the manufacturer's instructions. In brief, 500 ng of total RNA was prepared, an oligo-dT primer containing an Illumina-compatible sequence at its 5' end was hybridized to the RNA, and reverse transcription was performed. After degradation of the RNA template, second-strand synthesis was initiated by a random primer containing an Illumina-compatible linker sequence at its 5' end. The double-stranded library was purified using magnetic beads to remove all the reaction components. The library was amplified to add complete adapter sequences required for cluster generation. The finished library was purified from the PCR components. High-throughput sequencing was performed as single-end 75 sequencing using a NextSeq 500 (Illumina, Inc., CA, USA).

Data analysis
QuantSeq 3 mRNA-Seq reads were aligned using Bowtie2 (Langmead and Salzberg, 2012). Bowtie2 indices were either generated from the genome assembly sequence or representative transcript sequences for alignment to the genome and transcriptome. The alignment file was used for assembling transcripts, estimating their abundance, and detecting differential gene expression. Differentially expressed genes were determined based on counts from unique and multiple alignments, using coverage in Bedtools. The read count data were processed based on the quantile normalization method using EdgeR within R (R Development Core Team, 2016) and Bioconductor (Gentleman et al., 2004). Gene classification was based on searches performed using the DAVID (http://david.abcc.ncifcrf.gov/) and Medline databases (http://www.ncbi.nlm.nih.gov/).

Quantification of ECM components
Masson trichrome staining
Masson's trichrome staining was performed for the histological visualization of collagen, which is an extracellular component and is considered a hindrance when transporting TRZ. Tumor tissues were obtained after sacrificing the animals after 1 week of LOS treatment. The tissues obtained were fixed in 4% paraformaldehyde overnight and transferred to an Optimal cutting temperature compound (OCT compound) (Sakura Finetec, USA). The tissues were sectioned at a thickness of 40 μm. Staining was performed according to the manufacturer's protocol (Abcam (www.abcam.com) ab150686; Abcam). Bouin's fluid was added to each section and incubated overnight at room temperature. The slides were rinsed in water and incubated in Wiegert's iron hematoxylin for 5 min, followed by a Biebrich scarlet/acid fuchsin solution for 15 min after rinsing with tap water. The slides were then differentiated in a phosphomolybdic/phosphotungstic acid solution for 30 min. The slides were incubated again with aniline blue for 30 min without rinsing. In the following steps, the slides were rinsed in water and incubated for 3–5 min in acetic acid. The sections were then dehydrated in graded alcohol, cleared in xylene, and mounted on a glass slide using a mounted medium. The slides were visualized, and images were taken with an Olympus BX53 system microscope (Olympus, Life Science Solution, Waltham, MA, USA).

Alcian blue stain
ECM polysaccharide staining was performed using an Alcian blue stain kit (Vector Laboratories, Burlingame, CA 94,010, Alcian Blue (pH 2.5), Stain kit, H-3501). The tissue was sectioned at 20-μm thickness. The sections were then washed with water to remove excess OCT. Acetic acid was applied to the tissue sections for 3 min, followed by alcian blue solution for 30 min at 37 °C. Excess stain was removed by rinsing with acetic acid. This was followed by 2 min of washing in tap water with two changes in distilled water (1–2 min). A nuclear fast red solution was applied for 5 min, rinsed in tap water, and then distilled water. The slides were then dehydrated in graded alcohol, cleared in xylene, and mounted on cover slips. The slides were visualized, and images were obtained using an Olympus BX53 system microscope (Olympus, Life Science Solution, Waltham, MA, USA).

Quantification of fraction of collagen and ECM polysaccharide
The fraction of collagen and/or ECM polysaccharides was quantified by k-means clustering using an in-house MATLAB program[33,34]. Briefly, the image of Masson's trichrome staining was imported and segmented4 into background and collagen and/or ECM polysaccharides (stained in blue). Then, the fraction of collagen and/or ECM polysaccharides was divided by the total area. The final result is represented as the fraction of collagen (%) and the fraction of ECM polysaccharide (%).

Measurement of interstitial fluid pressure (IFP)
In vivo IFP was measured using a Millar Mikro-Tip pressure catheter transducer (SPR-1000, 0.33 mm diameter). Catheter transducers possess a shielded side-mounted sensor and can measure pressures ranging from 50 to 300 mmHg. For pressure recording, the catheter was first connected to a PCU-2000 control unit and an AD Instruments Power Lab data acquisition system (Millar Instruments, Inc. TX, USA). The pressure catheter was first inserted into the middle part of the 25- gauge needle, and the needle was then directly inserted into the tumor. Subsequently, the catheter probe was moved forward into the space and the needle was retracted. The readings were recorded at three different points from the tumor samples of the control group (n = 4), LOS group (n = 3), and ^{64}Cu-TRZ and ^{64}Cu-TRZ plus LOS groups (each n = 4), and were further analyzed using LabChart software (Millar Instruments, Inc., TX, USA). Prior to the experiment, the system was calibrated to 0.25 and 100 mmHg for each reading according to manual instructions.

Penetration and distribution studies
The groups for penetration and distribution studies comprised two groups of five mice each. Groups 1 and 2 received 150 μg TRZ conjugated to Alexa-647 with or without LOS and LOS was intraperitoneally injected at 40 mg/kg for 5 days.

Radiolabeling of ^{64}Cu-DOTA-Trastuzumab
TRZ (20 mg) was mixed with 1 mg of DOTA-NHS-ester (Macrocyclics, USA) in 0.1 M sodium bicarbonate buffer, pH 8.5. The conjugates were allowed to proceed with mild shaking at 4 °C overnight and separated from the non-conjugated chelates using a PD-10 column eluted with 1 mM sodium acetate buffer (pH 6.5). ^{64}CuCl$_2$ (370 MBq) was added to 1 mg DOTA-TRZ in 1 mM sodium acetate (pH 5.5) and incubated for 1 h at 37 °C. ^{64}Cu-DOTA-TRZ was purified on a PD-10 column and eluted with 1 mM sodium acetate buffer. The radiochemical purity was ≥ 98%, based on ITLC analysis.

PET/CT images of ^{64}Cu-DOTA-Trastuzumab
PET/CT images were acquired using a Siemens Inveon PET scanner (Siemens Medical Solutions, PA, USA). When the tumor size reached 200 mm^3 on average, ^{64}Cu-DOTA-TRZ (150 μg, 5.5 MBq/ 200 μL) was injected intravenously, with or without LOS for 5 days. PET/CT was performed at 4 h, 12 h and on days 2, 3, 4, and 5. The 24 and 48 h PET/CT was carried out for tumor tissue treated with siSERPINE1 or NC. The mice were anesthetized using 2.5% isoflurane, and PET data were acquired at a 15 min scan time with an energy window of 350–650 keV. OSEM2D reconstruction algorithms were applied to reconstruct the PET data with a matrix size of 128 × 128 × 159. The voxel size was 0.776 mm × 0.776 mm × 0.796 mm. CT images were acquired for 15 min after PET with full rotation and 180° projection using an Inveon system. Inveon Research Workflow software was used for image visualization and quantification.

Therapeutic efficacy studies

For therapeutic efficacy studies, groupings were classified as ^{64}Cu-TRZ (n = 7), ^{64}Cu-TRZ with LOS (n = 7), LOS alone (n = 6), TRZ alone (n = 6), and PBS (n = 8). The treatment plan included 5.5 MBq/150 μg of ^{64}Cu-TRZ with or without LOS. LOS was delivered intraperitoneally for 25 days, and TRZ (150 μg) was intravenously injected once at the start of treatment. Tumor growth was monitored, and tumor volume was calculated using the formula: width^2 × length × 0.5.

In Vitro immunofluorescence staining for alexa-647-trastuzumab binding

NCI-N87 cells were seeded in a 6-well plate at a density of 5×10^5 cells per well. The cells were then washed, fixed in 4% PFA, and treated with free Alexa Fluor-647 NHS Ester (1 mg, Invitrogen, USA) and Alexa Fluor-647 conjugated TRZ. The cells were washed with PBS and counterstained using Prolong Gold antifade reagent with 4, 6-diamidino-2-phenyindole (DAPI) (Invitrogen, USA). Images were acquired using cell microscopes for the respective channels: DAPI for nuclei (blue, Ex/Em = 358 / 461 nm) and Cy5 for Alexa-647-TRZ (green, Ex/Em = 594/633 nm). Fluorescent images were acquired with a 10 × objective using an in-cell analyzer (n cell analyzer 2200; GE Healthcare, Uppsala, Sweden) equipped with mosaic stitching software (Cell Developer Toolbox; GE Healthcare).

Immunofluorescence staining

To attain tumor sizes of 200 ± 20 mm^3, Alexa-647-TRZ (150 μg in 100 μL of PBS) was intravenously injected into NCI-N87 bearing mice, and LOS (40 mg/kg) was injected for 5 days. Five days after the injection of Alexa-647-TRZ, rhodamine-lectin (Rhodamine Ricinus Communis Agglutinin I, 1 mg in 200 μL of PBS) was injected intravenously into tumor-bearing mice. The mice were euthanized via CO_2 inhalation after 10 min of rhodamine-lectin administration and exsanguinated via cardiac puncture before dissection. Ex-vivo samples were stained with SERPINE1 antibody (ab66705, Abcam, UK) and anti-rabbit Alexa Flour-647 goat secondary antibody (ab150079, Abcam, UK).

The tumors were isolated and fixed with 4% paraformaldehyde overnight at 4 °C. The tumors were dehydrated with 30% sucrose in PBS solution until the tissue sank to the bottom of the tube at 4 °C, then frozen in OCT compound (Sakura Finetec, USA). Frozen tumors were sectioned at 8-μm thickness using a cryostat microtome (CM1800; LEICA Instruments) in three different cross-sectional areas each (25%, 50%, and 75% from the tumor apex). Next, seven sections were randomly selected from each cross-sectional area of three different tumors (n = 3). Tumor sections were fixed with 4% paraformaldehyde for 10 min, washed with PBS three times for 5 min, and mounted using Prolong Gold antifade reagent with DAPI (Invitrogen, USA).

Acquisition and analysis of fluorescent images

Fluorescent images were acquired with a 10 × objective using an In Cell Analyzer (In Cell Analyzer 2200, GE Healthcare, Upp sala, Sweden) equipped with mosaic stitching software (In Cell Developer Toolbox, GE Healthcare). Three independent channels were obtained: DAPI for nuclei (blue, Ex/Em = 358/461 nm), rhodamine for blood vessels (red, Ex/Em = 558/581 nm), and Cy5 for Alexa-647-TRZ (green, Ex/Em = 594/633 nm). Image analysis was performed using an in-house program written in MATLAB (MathWorks, Natick, MA, USA), ZEN (blue), and MIPAV (National Institutes of Health, Bethesda, MD, USA), as previously described [3] Briefly, TIFF files were exported and read by plotting a line graph using the MIPAV software. TRZ intensity was calculated by reading the images from the edge vessel, which drew the volume of interest (VOI). The total accumulation was calculated by drawing the region of interest (ROI) across the entire tumor. The area under the curve (AUC) was calculated and is shown on the graph. The total Alexa-647-TRZ accumulation was calculated as follows: total tumor intensity of mAb = intensity of mAb in the tumor/total tumor area.

Quantitative real-time polymerase chain reaction (qPCR)

Total RNA was extracted from the cells using TRIzol (Molecular Research Center, USA) according to the manufacturer's instructions. The tumors were cut into small portions using scissors. TRIzol reagent was added to the tissues, which were then incubated for 5 min at room temperature. The tissues were then lysed using a homogenizer. Total RNA was extracted from the lysed tissue samples. Isolated RNA was quantified using a NanoDrop spectrophotometer and diluted in RNase-free dH_2O (Thermo Fisher Scientific, MA, USA). To generate cDNA from 5 μg of mRNA, a Superscript III cDNA Synthesis Kit (Invitrogen) was used according to the manufacturer's instructions. Using SYBR Green PCR Master Mix (Applied Biosystems, MA, USA), qPCR was performed on an ABI qPCR system (Applied Biosystems) according to the manufacturer's instructions. The reaction conditions were as follows: 10 min at 95 °C and 50 cycles at 95 °C for 15 s and at 60 °C for 60 s. The following primer sequences were used: GAPDH forward: GCCTCAAGATCATCAGCAATGCCT; reverse: TGTGGTCATGAGTCCTTCCACGAT; MMP2 forward: AAAACGGACAAAGAGTTGGCA; reverse: CTGGGGCAGTCCAAAGAACT; TGFβ1 forward: CCGTGGAGGGGAAATTGAGG, Reverse: GTAGTGAACCCGTTGATGTCCA. The mRNA values were normalized to that of the housekeeping gene GAPDH. Relative quantity (RQ) values for mRNA expression were calculated using the following equation RQ = $2^{-\Delta\Delta Ct}$.

The human protein atlas

Interactive survival plot and survival analysis was obtained from the human protein atlas database (Stomach cancer TCGA) for SERPINE1 gene. The survival analysis for high and low expression SERPINE1 was conducted at cut off value of 24.7[35].

Western blot

Protein extracts were generated from fresh frozen tumor tissue following tissue homogenization with RIPA lysis buffer and Protease/Phosphatase Inhibitor (Thermo Fisher Scientific, USA). The protein concentrations in the lysates were measured using a BSA assay kit (Thermo Fisher Scientific, MA, USA), and proteins were further separated by 10% Tris–glycine gel electrophoresis and transferred to nitrocellulose membranes using a Blot 2 Dry Blotting System (Thermo Fisher Scientific, MA, USA). The membranes were blocked with 5% (w/v) non-fat dried milk in Tris-buffered saline containing 0.05% Tween 20 (TBST) and incubated with the appropriate antibodies. Primary antibodies against SERPINE1 antibody (ab66705, Abcam, UK) were used at a 1:1000 dilution (5% bovine serum albumin) and beta-actin (ab6276, Abcam, UK) at a 1:5000 dilution (5% skim milk). Membranes were incubated overnight and then treated with an HRP-conjugated secondary antibody. Immunoreactive protein bands were visualized using an enhanced chemiluminescence (ECL) reaction (Thermo Fisher Scientific, MA, USA) Amersham Imager 600 (GE Healthcare Life Sciences, NJ, USA) and scanned. Quantitative results were obtained using ImageJ in the form of bar graphs. Raw images were shown in **Fig S6**.

Transfection

The three siRNA inhibitor siRNA#1, (F: RNA-CUA AUC AGC CCA CCA UGU U = tt(4-AS, R: RNA-AAC AUG GUG GGC UGA UUA G = tt(4-AA)), siRNA#2 (F: RNA-GAG AGA AAG AGA ACU ACU A = tt(5-AS), R: UAG UAG UUC UCU UUC UCU C = tt(5-AA), siRNA#3 (F: RNA-CAC ACA AAA GGU AUG AUC A = tt(6-AS), R: UGA UCA UAC CUU UUG UGU G = tt(6-AA) were purchased from Bioneer (Korea). NCI-N87 cells were seeded into culture dishes and transfected with the siRNA inhibitors for SERPINE1 using Lipofectamine 2000 (Invitrogen) according to the manufacturer's instructions. NC represented negative control with nonspecific targeting siRNA delivery. siRNA#3 showed the dominant silencing of the SERPINE1. We used siRNA#3 in our study.

MMP activity assay

Ex-vivo tumor tissue protein extracts were quantified for protein concentration using a BSA assay kit (Thermo Fisher Scientific, MA, USA). MMP activity in the tumor tissue was quantified using an MMP activity assay kit (Fluorometric Green) (ab112146,UK). After complete thawing of the kit reagents, A 2 mM APMA working solution was prepared at a 1:500 dilution in assay buffer. Equal volume of sample and the working solution were loaded into the black 96-well plates. The enzymatic reaction was performed by incubating the plate overnight at 37 °C. The MMP green substrate working solution was prepared with assay buffer at 1:100 dilution, and 50 μL was added to each sample well. The reaction was incubated for 60 min for end-point reading. Fluorescence intensity was recorded using a microplate reader (i3X, Molecular Devices, CA, USA) at Ex/Em = 490/525 nm.

Statistical analysis

All statistical analyses were performed using PRISM software (version 5.0, GraphPad Software; San Diego, CA, USA). Data are expressed as the mean ± SD. Normality tests were performed using both the D'Agostino-Pearson omnibus normality test and Shapiro–Wilk normality test. Group comparisons were performed using unpaired two-tailed Student's t-test. When the normality test failed, the Mann–Whitney Wilcoxon test was performed. One way Anova test and the log-rank (Mantel-Cox) test was performed to compare tumor volume and the survival rates. * denotes $P < 0.05$, ** denotes $P < 0.005$, *** denotes $P < 0.001$.

Data availability

References

1. Etemadi, A. et al. The global, regional, and national burden of stomach cancer in 195 countries, 1990–2017: A systematic analysis for the Global Burden of Disease study 2017. *Lancet Gastroenterol. Hepatol.* **5**, 42–54. https://doi.org/10.1016/S2468-1253(19)30328-0 (2020).
2. Meza-Junco, J., Au, H. J. & Sawyer, M. B. Trastuzumab for gastric cancer. *Expert Opin. Biol. Ther.* **9**, 1543–1551. https://doi.org/10.1517/14712590903439702 (2009).
3. Zaheer, J., Kim, H., Lee, Y. J., Lim, S. M. & Kim, J. S. Comparison between Fractionated Dose and Single Dose of Cu-64 Trastuzumab Therapy in the NCI-N87 Gastric Cancer Mouse Model. *Int. J. Mol. Sci.* https://doi.org/10.3390/ijms20194708 (2019).
4. Jung, B. K. et al. Relaxin-expressing oncolytic adenovirus induces remodeling of physical and immunological aspects of cold tumor to potentiate PD-1 blockade. *J. Immunother. Cancer* https://doi.org/10.1136/jitc-2020-000763 (2020).
5. Zaheer, J., Kim, H., Lee, Y.-J., Kim, J. S. & Lim, S. M. Combination Radioimmunotherapy Strategies for Solid Tumors. *Int. J. Mol. Sci.* **20**, 5579 (2019).
6. Kim, J. S. Combination radioimmunotherapy approaches and quantification of Immuno-PET. *Nucl. Med. Mol. Imaging* **50**, 104–111. https://doi.org/10.1007/s13139-015-0392-7 (2016).
7. Chauhan, V. P. et al. Angiotensin inhibition enhances drug delivery and potentiates chemotherapy by decompressing tumour blood vessels. *Nat. Commun.* **4**, 2516. https://doi.org/10.1038/ncomms3516 (2013).
8. Diop-Frimpong, B., Chauhan, V. P., Krane, S., Boucher, Y. & Jain, R. K. Losartan inhibits collagen I synthesis and improves the distribution and efficacy of nanotherapeutics in tumors. *Proc. Natl. Acad. Sci. U S A* **108**, 2909–2914. https://doi.org/10.1073/pnas.1018892108 (2011).

9. Netti, P. A., Berk, D. A., Swartz, M. A., Grodzinsky, A. J. & Jain, R. K. Role of extracellular matrix assembly in interstitial transport in solid tumors. *Cancer Res* **60**, 2497–2503 (2000).
10. Zhao, Y. et al. Losartan treatment enhances chemotherapy efficacy and reduces ascites in ovarian cancer models by normalizing the tumor stroma. *Proc. Natl. Acad. Sci.* **116**, 2210–2219. https://doi.org/10.1073/pnas.1818357116 (2019).
11. Yang, Z. et al. Extracellular matrix characterization in gastric cancer helps to predict prognosis and chemotherapy response. *Front. Oncol.* **11**, 753330. https://doi.org/10.3389/fonc.2021.753330 (2021).
12. Eikenes, L., Bruland, Ø. S., Brekken, C. & Davies, C. D. L. Collagenase increases the transcapillary pressure gradient and improves the uptake and distribution of monoclonal antibodies in human osteosarcoma xenografts. *Cancer Res.* **64**, 4768–4773. https://doi.org/10.1158/0008-5472.Can-03-1472 (2004).
13. Brekken, C., Hjelstuen, M. H., Bruland, Ø. S. & de Lange, D. C. Hyaluronidase-induced periodic modulation of the interstitial fluid pressure increases selective antibody uptake in human osteosarcoma xenografts. *Anticancer Res.* **20**, 3513–3519 (2000).
14. Mok, W., Boucher, Y. & Jain, R. K. Matrix metalloproteinases-1 and -8 improve the distribution and efficacy of an oncolytic virus. *Cancer Res.* **67**, 10664–10668. https://doi.org/10.1158/0008-5472.Can-07-3107 (2007).
15. Larson, S. M., Carrasquillo, J. A., Cheung, N. K. & Press, O. W. Radioimmunotherapy of human tumours. *Nat. Rev. Cancer* **15**, 347–360. https://doi.org/10.1038/nrc3925 (2015).
16. Yang, J.-D., Ma, L. & Zhu, Z. SERPINE1 as a cancer-promoting gene in gastric adenocarcinoma: facilitates tumour cell proliferation, migration, and invasion by regulating EMT. *J. Chemother.* **31**, 408–418. https://doi.org/10.1080/1120009X.2019.1687996 (2019).
17. Xu, B., Bai, Z., Yin, J. & Zhang, Z. Global transcriptomic analysis identifies SERPINE1 as a prognostic biomarker associated with epithelial-to-mesenchymal transition in gastric cancer. *PeerJ* **7**, e7091. https://doi.org/10.7717/peerj.7091 (2019).
18. Jabłońska-Trypuć, A., Matejczyk, M. & Rosochacki, S. Matrix metalloproteinases (MMPs), the main extracellular matrix (ECM) enzymes in collagen degradation, as a target for anticancer drugs. *J. Enzyme Inhibition Med. Chem.* **31**, 177–183. https://doi.org/10.3109/14756366.2016.1161620 (2016).
19. Aimes, R. T. & Quigley, J. P. Matrix metalloproteinase-2 is an interstitial collagenase. Inhibitor-free enzyme catalyzes the cleavage of collagen fibrils and soluble native type I collagen generating the specific 3/4- and 1/4-length fragments. *J. Biol. Chem.* **270**, 5872–5876. https://doi.org/10.1074/jbc.270.11.5872 (1995).
20. Huang, Y. et al. RNF12 is regulated by AKT phosphorylation and promotes TGF-β driven breast cancer metastasis. *Cell Death Dis.* **13**, 44. https://doi.org/10.1038/s41419-021-04493-y (2022).
21. Yoon, H. et al. TGF-β1-mediated transition of resident fibroblasts to cancer-associated fibroblasts promotes cancer metastasis in gastrointestinal stromal tumor. *Oncogenesis* **10**, 13. https://doi.org/10.1038/s41389-021-00302-5 (2021).
22. Heine, M. et al. High Interstitial fluid pressure is associated with low Tumour Penetration of Diagnostic Monoclonal Antibodies applied for molecular imaging purposes. *PLoS ONE* **7**, e36258. https://doi.org/10.1371/journal.pone.0036258 (2012).
23. Kim, H. G. et al. Measurement of tumor pressure and strategies of imaging tumor pressure for radioimmunotherapy. *Nucl. Med. Mol. Imaging* **53**, 235–241. https://doi.org/10.1007/s13139-019-00598-7 (2019).
24. Heldin, C. H., Rubin, K., Pietras, K. & Ostman, A. High interstitial fluid pressure - an obstacle in cancer therapy. *Nat. Rev. Cancer* **4**, 806–813. https://doi.org/10.1038/nrc1456 (2004).
25. Khaibullina, A. et al. Pulsed High-Intensity Focused Ultrasound Enhances Uptake of Radiolabeled Monoclonal Antibody to Human Epidermoid Tumor in Nude Mice. *J. Nucl. Med.* **49**, 295–302. https://doi.org/10.2967/jnumed.107.046888 (2008).
26. Jang, B. S. et al. Combined-modality radioimmunotherapy: synergistic effect of paclitaxel and additive effect of bevacizumab. *Nucl. Med. Biol.* **39**, 472–483. https://doi.org/10.1016/j.nucmedbio.2011.10.020 (2012).
27. Wang, S. et al. Pulsed high intensity focused ultrasound increases penetration and therapeutic efficacy of monoclonal antibodies in murine xenograft tumors. *J Control Release* **162**, 218–224. https://doi.org/10.1016/j.jconrel.2012.06.025 (2012).
28. Lu, Y. & Wang, W. Interaction between the interstitial fluid and the extracellular matrix in confined indentation. *J. Biomech. Eng.* **130**, 041011. https://doi.org/10.1115/1.2939310 (2008).
29. Boucher, Y. & Jain, R. K. Microvascular pressure is the principal driving force for interstitial hypertension in solid tumors: implications for vascular collapse. *Cancer Res* **52**, 5110–5114 (1992).
30. Salnikov, A. V. et al. Lowering of tumor interstitial fluid pressure specifically augments efficacy of chemotherapy. *Faseb j.* **17**, 1756–1758. https://doi.org/10.1096/fj.02-1201fje (2003).
31. Reed, R. K. & Rubin, K. Transcapillary exchange: role and importance of the interstitial fluid pressure and the extracellular matrix. *Cardiovas. Res.* **87**, 211–217. https://doi.org/10.1093/cvr/cvq143 (2010).
32. Zhou, X., Hendrickx, M. L., Hassanzadeh-Ghassabeh, G., Muyldermans, S. & Declerck, P. J. Generation and in vitro characterisation of inhibitory nanobodies towards plasminogen activator inhibitor 1. *Thromb. Haemost* **116**, 1032–1040. https://doi.org/10.1160/th16-04-0306 (2016).
33. Zhang, Y. et al. Automatic segmentation of intravital fluorescence microscopy images by K-means clustering of FLIM phasors. *Opt. Lett.* **44**, 3928–3931. https://doi.org/10.1364/OL.44.003928 (2019).
34. Irrgang, J., Ksienczyk, J., Lapiene, V. & Niemeyer, C. M. Analysis of Non-Covalent Bioconjugation of Colloidal Nanoparticles by Means of Atomic Force Microscopy and Data Clustering. *Chem. Phys. Chem.* **10**, 1483–1491. https://doi.org/10.1002/cphc.200800693 (2009).
35. Uhlén, M. et al. Tissue-based map of the human proteome. *Science* **347**, 1260419. https://doi.org/10.1126/science.1260419 (2015).

Author contributions

Conceptualization, J.S.K.; Experiment, J,Z.,J.S.,S.K.,H.K.; writing-original draft preparation, J.Z.; writing review and editing, J.S.K.; funding acquisition, J.S.K.; proofreading, J.S.K.

Funding

Declarations

Competing interests

The authors declare no conflict of interest. The funders had no role in the study design, collection, analysis, interpretation of data, writing of the manuscript, or in the decision to publish the results.

Ethical approval and consent to participate

Ethical approval and consent to participate: All experiments were performed under a protocol approved by the IACUC (approval number: KIRAMS 2020–0027) of the Korea Institute of Radiological and Medical Sciences (KIRAMS). The study is reported in accordance with ARRIVE guidelines.

Additional information

Supplementary Information The online version contains supplementary material available at https://doi.org/10.1038/s41598-025-97983-4.

Correspondence and requests for materials should be addressed to J.S.K.

Reprints and permissions information is available at www.nature.com/reprints.

Publisher's note Springer Nature remains neutral with regard to jurisdictional claims in published maps and institutional affiliations.